Available online at www.sciencedirect.com
ScienceDirect
Nuclear Physics B Proceedings Supplement 00 (2014) 1–6
Nuclear Physics B Proceedings Supplement

Measurements of Photon and Diphoton production cross-sections at CMS

Andrea Carlo Marini[a], on behalf of the CMS Collaboration

[a]*Institute for Particle Physics, ETH Zürich*

Abstract

The differential cross-section measurements of inclusive photon production, photon+jet production, diphoton production, and the differential cross-section ratio of Z/γ^*+jet over γ+jet in proton-proton (pp) collisions based on data recorded by the CMS detector at the LHC are presented. The associated production of a photon and one or more jets in pp collisions represents a direct probe of the hard QCD interaction, is sensitive to gluon densities in the proton and is a major source of background to Standard Model searches. The measured distributions, corrected for efficiencies and unfolded to generator level, are compared with theoretical predictions.

Keywords: photon, diphoton, gamma, Z, CMS

1. Introduction

The differential cross-section measurements of inclusive photon production, photon+jet production at 8 TeV, the diphoton production at 7 TeV, and the differential cross-section ratio of Z/γ^*+jet over γ+jet at 8 TeV based on data recorded by the CMS [1] detector are presented.

The measurement of the photon production cross-section represents a very sensitive test of perturbative quantum chromodynamics (pQCD). The main contribution to the photon production in pp collisions at the LHC energies (7 TeV, 8 TeV) is the quark-gluon (qg) Compton-scattering at leading order (LO). Nevertheless, some region of the phase space receive important contributions from fragmentation photons, and the annihilation terms.

Photons represent a source of background for several new physics searches. Measuring the cross-section ratio differentially in p_{T} of the Z+jet over the γ+jet processes, allows to establish the existence of a plateau, that it is supposed to be reached in the ultrarelativistic range, where $p_{\mathrm{T}}^{Z} \gg m^{Z}$ [2]. This plateau is sensitive to the parton distribution functions (pdf) composition and it is used in new physics searches to evaluate the irreducible background of invisible decays of the Z-boson. The $Z \to \ell\ell$ is a proxy for calibration of the $Z \to \nu\bar{\nu}$ process, and γ+jet is used to extrapolate the Z spectrum where the leptonic decays of the Z don't have enough statistics, like high p_{T} or high H_{T}. High order quantum chromodynamics (QCD) and/or electroweak (EW) corrections may induce deviation from the flatness of the plateau, making this measurement useful also for higher order Monte Carlo generators.

Some regions of the diphoton production phase-space are essentially forbidden at the lowest order in perturbative expansion (e.g. low diphoton invariant mass region). Its large sensitivity to the next-to-leading order (NLO) and next-to-next-to-leading-order (NNLO) contributions makes it an important source of experimental input for the pQCD calculations.

2. Background Estimation

The main difficulty in performing a photon analysis resides in the background evaluation. The main source of background is the decays of neutral hadrons to pair of collimated photons that are reconstructed as a single electromagnetic cluster in the calorimeter.

The evaluation of this background relies on two classes of variables: isolations and shower-shapes. The isolation variables integrates the energy deposited

around the photon object. Thanks to the excellent performance of the particle flow event reconstruction [3], it is possible to perform the computation of the isolation separating the contribution of charged particles, neutral hadrons, and soft photon candidates. The shower-shape variables aims to characterize the photon electromagnetic shower. The variable used in this analysis is $\sigma_{i\eta i\eta}$ [4], which measures the extension of the shower in pseudorapidity with the energy weighted spread within the 5x5 crystal matrix around the most energetic crystal.

The signal and the background event yields are determined by template fits to the isolation distributions. A dedicated technique has been developed to extract both the signal and background templates from data.

The signal template is constructed using the random-cone technique: for each selected photon, the particle-flow isolation variable, removing the foot-print of the photon, is calculated both around the photon candidate, and in an "empty" region of detector, chosen by rotating the isolation cone at the same pseudorapidity [5]. The region is checked to be free from hard objects like jets above a given threshold. Figure 1 shows data - Monte Carlo agreement for the signal templates obtained with the random-cone.

The data-driven estimation of the background template is performed inverting the shower-shape requirement on the $\sigma_{i\eta i\eta}$ variable (see figure 1).

The difference between the templates extracted using Monte Carlo truth information and the ones extracted from applying the methods to simulated objects, and the small correlations between the shower-shape and isolation variables, are considered as systematic uncertainties of this method.

For the diphoton measurements a two-dimensional fit is performed to correctly take into account the correlation induced by the pile-up activity in the two photon isolation cones.

3. Diphoton Results at 7 TeV

The results of the diphoton differential cross-section measurements are presented in figure 2 [5], the invariant mass of the diphoton system is shown ($m_{\gamma\gamma}$), its transverse momentum ($p_T^{\gamma\gamma}$) and the azimuthal angle between the two photons ($\Delta\phi_{\gamma\gamma}$). Results are compared to DIPHOX+GAMMA2MC [6, 7], 2γNNLO [8], SHERPA [9], and RESBOS [10]. An asymmetric requirement on the transverse momentum of the two photons($p_{\mathrm{T}}^{\gamma_1} > 40$GeV, $p_{\mathrm{T}}^{\gamma_2} > 25$GeV), induces the kink visible in the $p_T^{\gamma\gamma}$ distribution. All differential distributions are well reproduced by the NNLO theory predictions.

4. Photon + jet at 8 TeV

The photon plus jet cross-section measurement is presented for the 8 TeV data [11]. The spectra are measured differentially in the number of jets and for different H_{T} requirements. The results are compared to MadGraph simulation (multi-leg LO). The slope is consistent with what observed for the Z+jet events (where the Z inclusive cross-section is taken from the NNLO predictions). Figure 3 shows the photon cross-section compared to Monte Carlo predictions for $N_{\mathrm{jets}} \geq 1$, and the Monte Carlo over data ratio for $N_{\mathrm{jets}} \geq 1$, $N_{\mathrm{jets}} \geq 2$, and $H_{\mathrm{T}} > 300$GeV.

The cross-section ratios with respect to the different number of jets are also presented. Figure 4 shows the differential cross-section ratio for $N_{\mathrm{jets}} \geq 2$ over the $N_{\mathrm{jets}} \geq 1$, and the data-MC ratio (for this ratio), as well as for the $N_{\mathrm{jets}} \geq 3/N_{\mathrm{jets}} \geq 2$.

5. Z+jet over photon+jet Cross section ratio

The measurement of the Z+jets over the photon+jets cross-section ratio, is presented differentially in p_T and N_{jets} and for different H_{T} requirements [11].

The cross-section ratio for $N_{\mathrm{jets}} \geq 1$, is presented together with data-MC comparison requiring $N_{\mathrm{jets}} \geq 2$, $H_{\mathrm{T}} > 300$GeV, and $N_{\mathrm{jets}} \geq 3$.

MadGraph correctly reproduces the shape of the Z+jet over photon+jet cross-section ratio, but it overestimated the integral value by about 20%. Within the present statistical uncertainty it also well describes the data even when applying different requirements on the extra hadronic activity in the event.

6. Conclusions

The photon+jet differential cross-section at $\sqrt{s} = 8$ TeV, the diphoton differential cross-section at 7 TeV, the cross-section ratios with increasing multiplicities in γ+jet events at 8 TeV, and the Z/γ^* over photon cross-section ratio differentially in the boson transverse momentum have been presented. The diphoton measurements shows the importance of the NNLO to correctly predict the diphoton cross-section especially at low invariant mass. The Z+jets to γ+jets cross-section ratio shows that the shape of the distribution is well predicted by multi-leg LO Monte Carlo, even though the total rate is overestimated by about 20%.

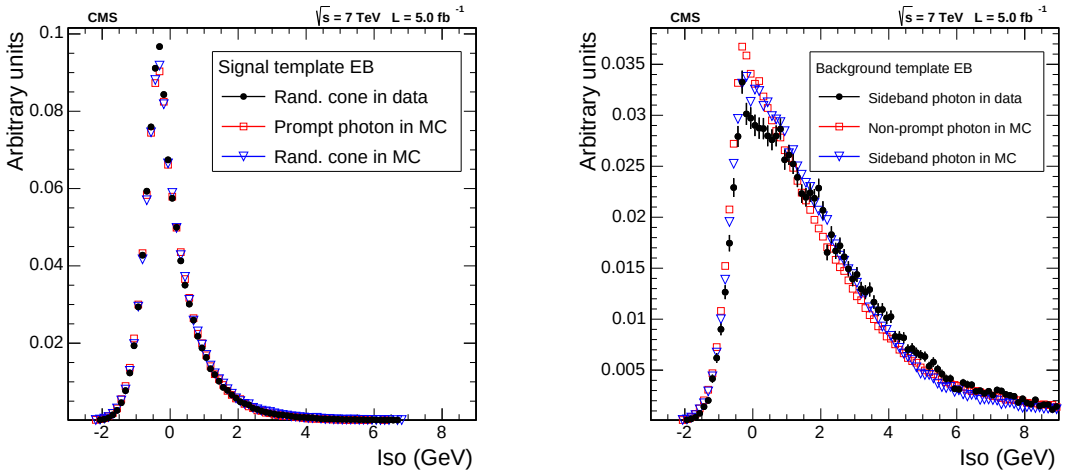

Figure 1: Left: Comparison of prompt photon (signal) templates in data and simulation: prompt photon in the simulations (squares), prompt photon templates extracted with the random cone technique from simulations (triangles) and from data (dots), for candidates in the ECAL barrel. Right: Comparison of non-prompt photon (background) templates in data and simulations: non-prompt photons in the simulations (squares), non-prompt photon templates extracted with the side-band technique from simulations (triangles) and from data (dots), for candidates in the ECAL barrel. All histograms are normalized to unit area.

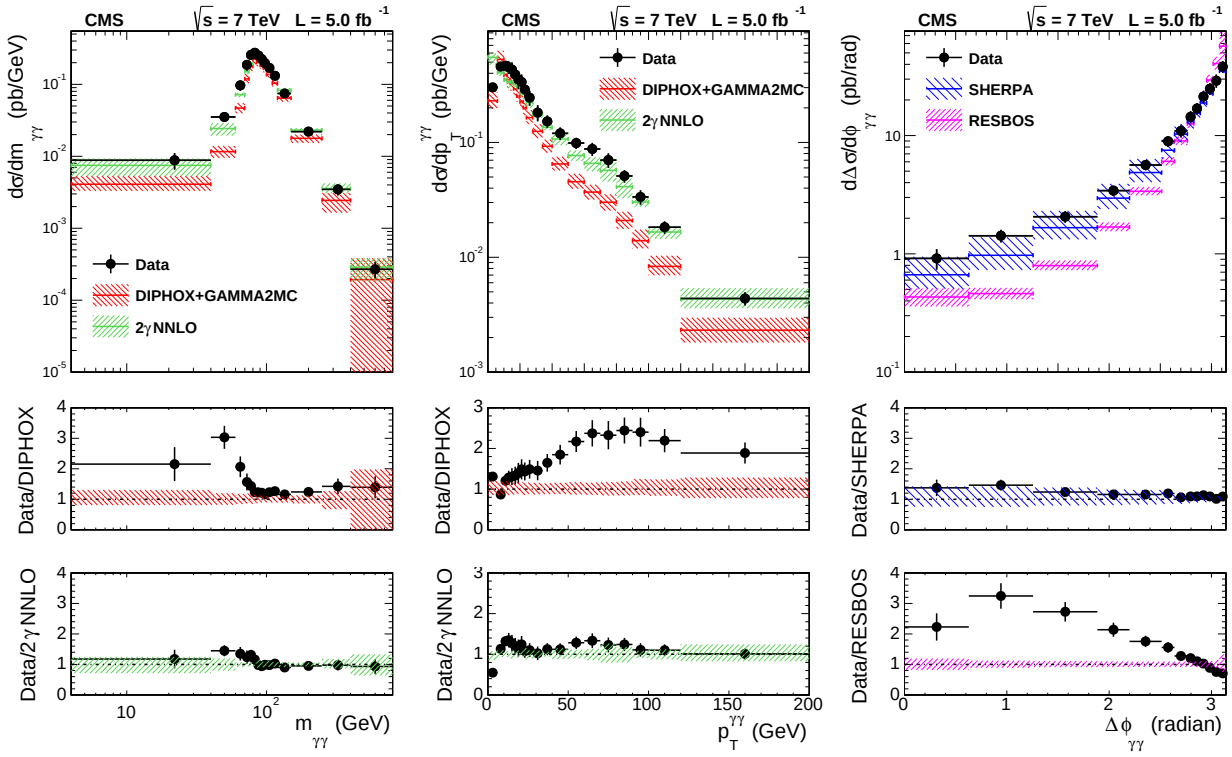

Figure 2: The comparisons of the differential cross-section between data and the DIPHOX + GAMMA2MC, and 2NNLO predictions. Black dots correspond to data with error bars including statistical and systematic uncertainties. Renormalization and factorization scale variations and PDF variations are included as systematics uncertainties in DIPHOX+GAMMA2MC. The same is done for 2gNNLO but neglecting the PDF variations.

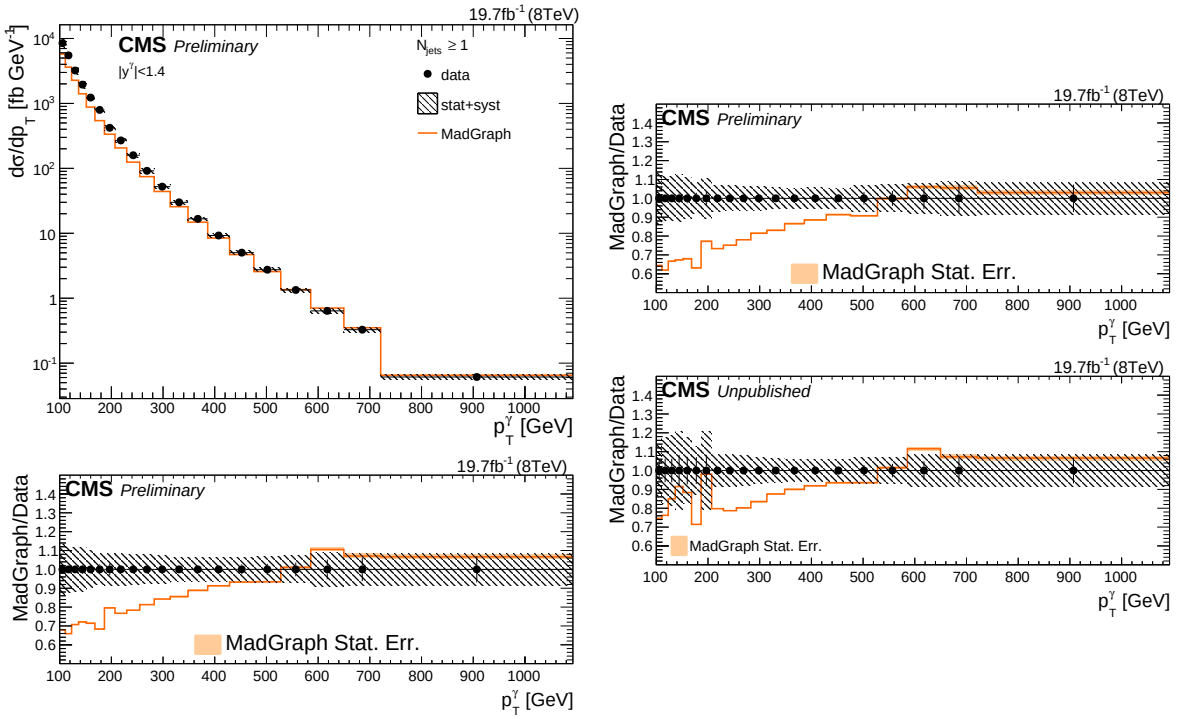

Figure 3: The γ differential transverse momentum cross-section in an inclusive γ + jets, $N_{\text{jets}} \geq 1$ (Left), $N_{\text{jets}} \geq 2$ (Right Top) and $H_{\text{T}} > 300$ GeV (Right Bottom) selections for central rapidity $|y_\gamma| < 1.4$ in data compared with prediction from MadGraph5.1.3.30+Pythia6.4.26. The hatched (grey) band represents the total uncertainty on the measurement, while the error bars show the statistical uncertainty. The shaded bands around MC/data ratios of MadGraph represent the statistical uncertainty of the MC prediction.

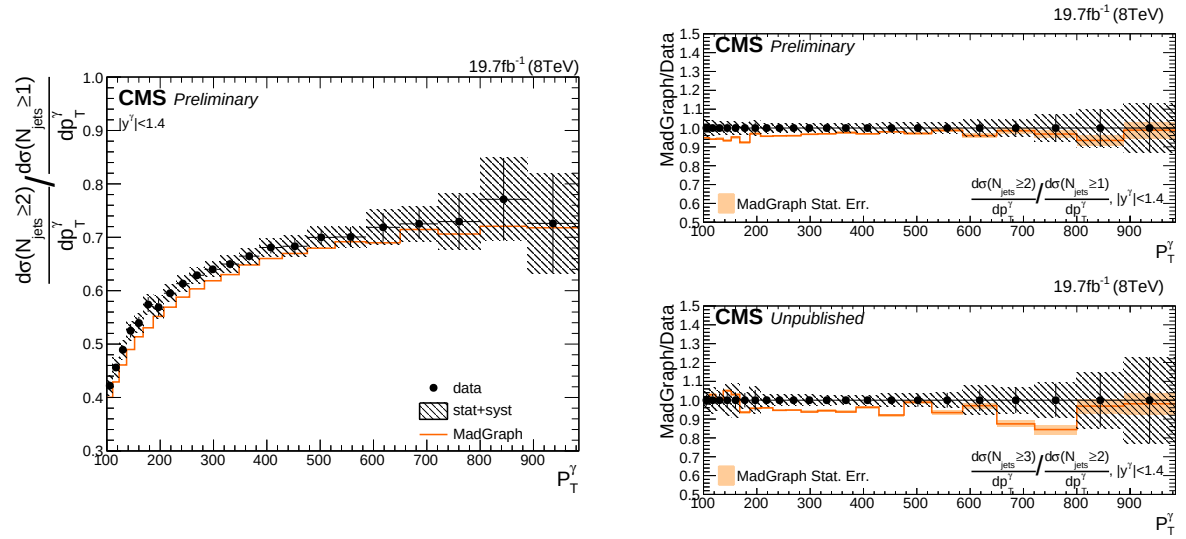

Figure 4: The ratio of the γ differential transverse momentum cross-section in an inclusive γ + jets, $N_{\text{jets}} \geq 2$ over γ + jets, $N_{\text{jets}} \geq 1$ and γ + jets, $N_{\text{jets}} \geq 3$ over γ + jets, $N_{\text{jets}} \geq 2$ selection for central rapidity $|y_\gamma| < 1.4$ in data compared with prediction from MadGraph5.1.3.30+Pythia6.4.26. The hatched (grey) band represents the total uncertainty on the measurement, while the error bars show the statistical uncertainty. The shaded bands around MC/data ratios of MadGraph and Sherpa represent the statistical uncertainty of the MC prediction.

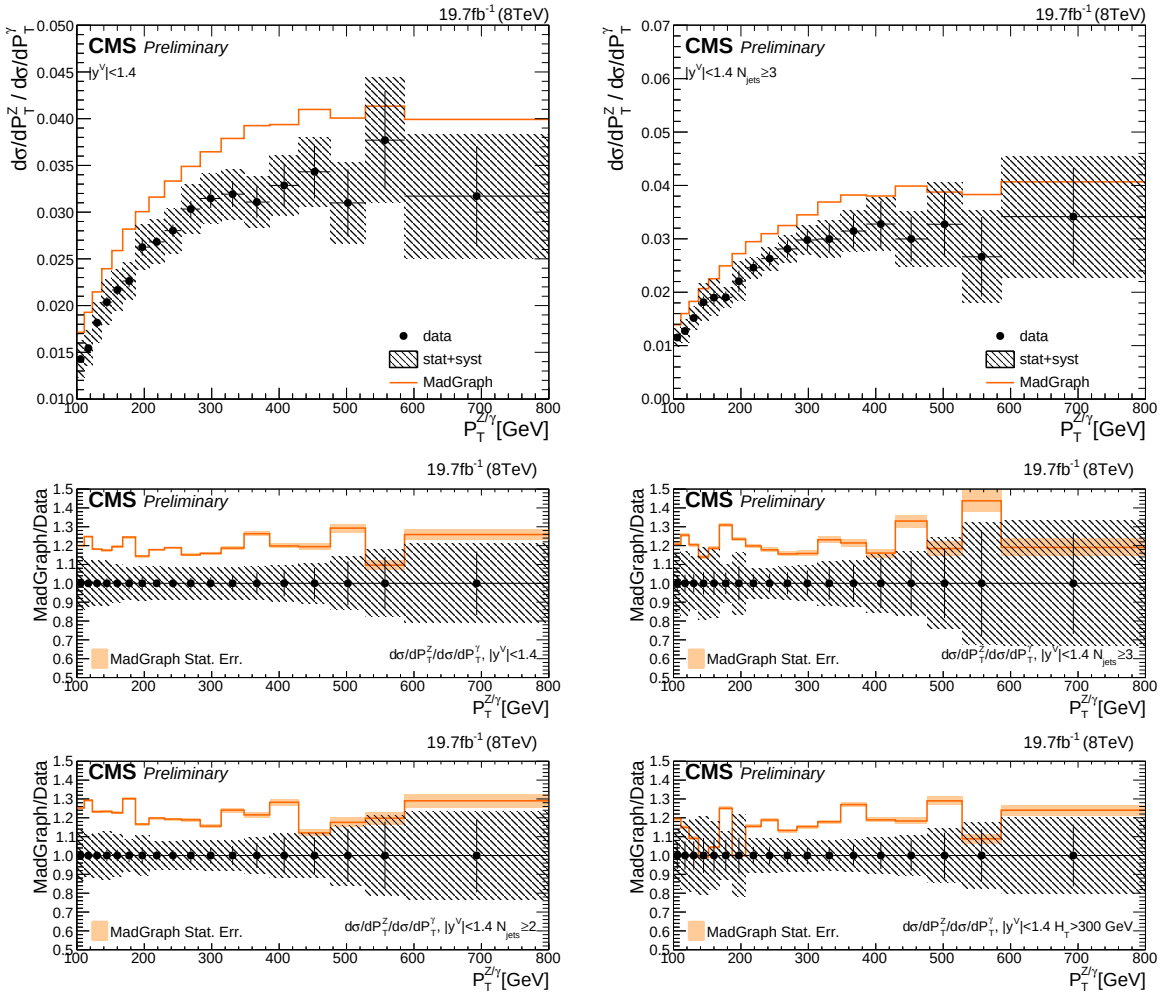

Figure 5: Differential cross-section ratio of leptonic Z over γ as a function of the total transverse momentum cross-section and for central bosons ($|y_V| < 1.4$), for the inclusive ($N_{\text{jets}} \geq 1$, Top Left), 2-jet ($N_{\text{jets}} \geq 2$, Bottom Left), 3-jet ($N_{\text{jets}} \geq 3$, Top right) and high H_{T} ($H_{\text{T}} > 300$ GeV, Bottom Right) selections. The black error bars reflect the statistical uncertainty of the ratio, the hatched (grey) band represents the total uncertainty of the measurement. The data points are compared to predictions from MadGraph5.1.3.30+Pythia6.4.26 using LO cross-sections for both processes. The shaded band around the MadGraph to data ratio represents the statistical uncertainty of the MC prediction.

References

[1] CMS Collaboration, The CMS experiment at the CERN LHC, JINST 03 (2008) S08004.

[2] S. Ask, M. A. Parker, T. Sandoval, M. E. Shea and W. J. Stirling, Using γ+jets Production to Calibrate the Standard Model $Z(\nu\nu)$+jets Background to New Physics Processes at the LHC, JHEP 10 (2011) 058. arXiv:1107.2803v2, doi:10.1007/JHEP10(2011)058.

[3] CMS Collaboration, Commissioning of the particle-flow event reconstruction with the first LHC collisions recorded in the CMS detector, CMS Physics Analysis Summary CMS-PAS-PFT-10-002 (2010).
URL http://cdsweb.cern.ch/record/1247373

[4] CMS Collaboration, Photon reconstruction and identification at $\sqrt{s}$ = 7TeV, CMS Physics Analysis Summary CMS-PAS-EGM-10-005 (2010).
URL https://cdsweb.cern.ch/record/1279143

[5] CMS Collaboration, Measurement of differential cross sections for the production of a pair of isolated photons in pp collisions at $\sqrt(s)$ = 7 TeV (2014). arXiv:1405.7225, submitted to Eur. Phys. J. C.

[6] T. Binoth, J. P. Guillet, E. Pilon, M. Werlen, A full next-to-leading order study of direct photon pair production in hadronic collisions, Eur. Phys. J. C 16 (2000) 311. arXiv:hep-ph/9911340, doi:10.1007/s100520050024.

[7] Z. Bern, L. J. Dixon, C. Schmidt, Isolating a light Higgs boson from the diphoton background at the CERN LHC, Phys. Rev. D 66 (2002) 074018. arXiv:hep-ph/0206194, doi:10.1103/PhysRevD.66.074018.

[8] S. Catani, L. Cieri, D. de Florian, G. Ferrera, M. Grazzini, Diphoton production at hadron colliders: a fully-differential QCD calculation at NNLO, Phys. Rev. Lett. 108 (2012) 072001. arXiv:1110.2375, doi:10.1103/PhysRevLett.108.072001.

[9] T. Gleisberg, S. Hoeche, F. Krauss, M. Schoenherr, S. Schumann, F. Siegert and J. Winter, Event generation with SHERPA 1.1, JHEP 0902 (2009) 007. arXiv:0811.4622, doi:10.1088/1126-6708/2009/02/007.

[10] C. Balázs, E. L. Berger, P. M. Nadolsky, C.-P. Yuan, Calculation of prompt diphoton production cross-sections at Tevatron and LHC energies, Phys. Rev. D 76 (2007) 013009. doi:10.1103/PhysRevD.76.013009.

[11] CMS Collaboration, Measurement of the ratio of the z/γ+jets and photon+jets cross section in pp collisions at $\sqrt{s}$ = 8 TeV, CMS Physics Analysis Summary CMS-PAS-SMP-14-005 (2010).
URL http://cds.cern.ch/record/1740969

[12] Johan Alwall, Michel Herquet, Fabio Maltoni, Olivier Mattelaer and Tim Stelzer, MadGraph 5: Going Beyond, JHEP 06 (2011) 128. arXiv:1106.0522, doi:10.1007/JHEP06(2011)128.

[13] Torbjorn Sjöstrand, Stephen Mrenna and Peter Skands, PYTHIA 6.4 Physics and Manual, JHEP 05 (2006) 026. arXiv:0603175, doi:10.1088/1126-6708/2006/05/026.

[14] CMS collaboration, Study of the underlying event at forward rapidity in pp collisions at $\sqrt{s}$ = 0.9, 2.76, and 7 TeV, JHEP 04 (2013) 072. arXiv:1302.2394, doi:10.1007_JHEP04(2013)072.

[15] J. Alwall, S. Hoeche, F. Krauss, N. Lavesson, L. Lonnblad, F. Maltoni, M.L. Mangano, M. Moretti, C.G. Papadopoulos, F. Piccinini, S. Schumann, M. Treccani, J. Winter, and M. Worek, Comparative study of various algorithms for the merging of parton showers and matrix elements in hadronic collisions, Eur. Phys. J. C 53 (2009) 473. arXiv:0706.2569, doi:10.1140/epjc/s10052-007-0490-5.

[16] J. Pumplin, D.R. Stump, J. Huston, H.L. Lai, P. Nadolsky, W.K. Tung, New Generation of Parton Distributions with Uncertainties from Global QCD Analysis, JHEP 0207 (2002) 12. arXiv:0201195, doi:10.1088/1126-6708/2002/07/012.

[17] Jun Gao, Marco Guzzi, Joey Huston, Hung-Liang Lai, Zhao Li, Pavel Nadolsky, Jon Pumplin, Daniel Stump, and C.-P. Yuan, CT10 next-to-next-to-leading order global analysis of QCD, Phys. Rev. D 89 (2014) 033009. arXiv:1302.6246, doi:10.1103/PhysRevD.89.033009.

[18] J. M. Campbell and R. K. Ellis, An update on vector boson pair production at hadron colliders, Phys. Rev. D 60 (1999) 113006. arXiv:9905386, doi:10.1103/PhysRevD.60.113006.

[19] Z. Bern, G. Diana, L. J. Dixon, F. Febres Cordero, S. Hoeche, H. Ita, D. A. Kosower, D. Maitre, K. J. Ozeren, Missing energy and jets for supersymmetry searches, Phys. Rev. D 87 (2013) 034026. arXiv:1206.6064, doi:10.1103/PhysRevD.87.034026.

[20] Z. Bern, L. J. Dixon, F. Febres Cordero, S. Hoeche, H. Ita, D. A. Kosower and D. Maitre, Ntuples for nlo events at hadron colliders, Comput. Phys. Commun. 5 (2014) 1443. arXiv:1310.7439, doi:10.1016/j.cpc.2014.01.011.

[21] A.D. Martin, W.J. Stirling, R.S. Thorne, G. Watt, Parton distributions for the LHC, Eur. Phys. J. C 63 (2009) 189. arXiv:0901.0002, doi:10.1140/epjc/s10052-009-1072-5.